# Holoscopy—holographic optical coherence tomography

**Dierck Hillmann,[1,2] Christian Lührs,[1,2] Tim Bonin,[1] Peter Koch,[2] and Gereon Hüttmann[1,*]**

[1]*Institute of Biomedical Optics, University of Lübeck, Peter-Monnik-Weg 4, 23562 Lübeck, Germany*

[2]*Thorlabs GmbH, Maria-Goeppert-Strasse 1, 23562 Lübeck, Germany*

**Corresponding author: huettmann@bmo.uni-luebeck.de*

Received January 24, 2011; revised April 22, 2011; accepted May 12, 2011;
posted June 6, 2011 (Doc. ID 141230); published June 20, 2011

Scanning optical coherence tomography (OCT) is limited in sensitivity and resolution by the restricted focal depth of the confocal detection scheme. Holoscopy, a combination of holography and Fourier-domain full-field OCT, is proposed as a way to detect photons from all depths of a sample volume simultaneously with uniform sensitivity and lateral resolution, even at high NAs. By using the scalar diffraction theory, as frequently applied in digital holographic imaging, we fully reconstruct the object field with depth-invariant imaging quality. *In vivo* imaging of human skin is demonstrated with an image quality comparable to conventionally scanned OCT. 

*OCIS codes:* 090.1995, 110.4500, 170.4500.

Scanning optical coherence tomography (OCT) is fundamentally limited by a degradation of the lateral resolution and a reduction of the sensitivity outside the focal region. With respect to these properties, the depth of field, which can be imaged with a single A scan, is limited to a few Rayleigh lengths $z_R = \lambda/(\pi \mathrm{NA}^2)$. The exact measuring depth depends on the acceptable image degradation. Scanning with multiple foci in different depths [1] and engineering of the point-spread function (PSF) [2] were demonstrated to increase the depth of field. Inverse scattering, which uses the amplitude and phase of the OCT data to correct for the blurring outside the focus provides a depth-independent lateral resolution [3–5], but still suffers from a reduced detection efficiency of photons that are scattered outside the Rayleigh range.

Eventually, imaging speed is restricted by the number of detected photons and thus exposure limits, and the efficiency of photon detection will ultimately determine the possible imaging speed. Assuming that confocal imaging detects only photons backscattered in the focal range (here approximated by twice the Rayleigh length $z_R$) and wide-field imaging collects photons from the complete accessible imaging depth $d$ of the sample, wide-field imaging is more effective by approximately $d/(2z_R) \approx \pi d \mathrm{NA}^2/(2\lambda)$. For a 3 mm depth range and an NA of 0.07, about 30 times more photons could be detected from a homogeneous sample.

Wide-field imaging with an area detector does not introduce a depth gating and is also sensitive to out-of-focus light. If the phase and amplitude of the scattered field are detected in wide-field imaging, either inverse scattering [6] or digital holography [7] can recover the image information outside the Rayleigh length and depth-independent resolution and sensitivity are possible. By combining Fourier-domain OCT with digital Fourier holography, which needs only a three-dimensional FFT for reconstruction, imaging within the Rayleigh length has been successfully demonstrated [8]. Going to the Fresnel region and adapting the reconstruction process, the imaging was extended to $10z_R$ for technical objects [9]. By summing reconstructions of digital holograms, which were recorded at around 50 wavelengths, depth-resolved *ex vivo* imaging of ocular structures and excised skin was presented over a few Rayleigh lengths, however with poor quality [10].

Here we propose holoscopy, the full combination of digital holography with FD-OCT, for photon-efficient imaging with constant sensitivity and lateral resolution over a depth, which is not limited by the NA. Holoscopy records digital holograms in an optical arrangement, in which the reference wave is matched with regard to propagation time and curvature to the imaging distance for optimal sampling of the interference pattern at a number of different wavelengths that is twice the number of pixels for the depth information. The recorded data are reconstructed by an efficient forward method, which blends holographic reconstruction by the angular spectrum approach [7] with the FFT-based A-scan calculation in FD-OCT.

The setup for holoscopy was a simple open Michelson interferometer consisting of a collimator, a beam splitter, and a convex spherical mirror with a focal length of $f = -10.34$ mm in the reference arm (Fig. 1). A convex mirror was chosen in order to reduce the spatial frequencies of the holograms in the camera plane, which are determined by the angle between the local reference and sample wavefront. Ideally, the reference wave would be a spherical wave with its origin as close as possible to the sample volume. A fast tunable light source (BroadSweeper BS-840-01, Superlum, Ireland) generated a wavelength sweep from 873.5 to 823.5 nm, which gave, after spectral

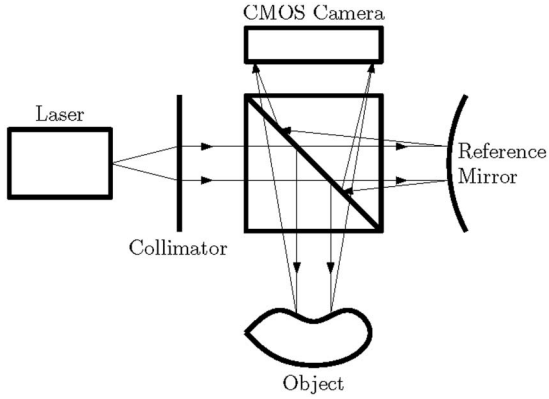


Fig. 1. Schematic setup of the holoscopy device.

 

shaping with a Hann window, a depth resolution of 14.7 $\mu$m in air. The instantaneous linewidth of the scanning laser source is specified with 50 pm. A drop in sensitivity of 6.8 dB (from 72 to 65.2 dB) over a depth of 3.6 mm was measured with this source in a full-field OCT configuration [11]. Thus we restricted the depth range for the holoscopic measurements to 3.8 mm in air. The acquisition sequence of 1024 frames was started by the start-of-scan trigger of the tunable laser and then recorded at a fixed frame rate. The object was placed without additional imaging optics directly in front of the beam splitter cube.

For *ex vivo* measurements, a 2.2 mm diameter collimated laser beam was used for sample illumination and the resulting interference pattern at the exit of the interferometer was detected by a fast CMOS camera (EoSens MC3010, Mikrotron GmbH, Germany) with $1696 \times 1710$ pixels of size $8\,\mu\text{m} \times 8\,\mu\text{m}$ each. For the measurements, a subregion of only $1024 \times 1024$ pixels was read out with an image acquisition speed of 440 fps. The tunable light source was adjusted to 20 nm/s for this measurement. The entire volume was thus recorded in 2.3 s, which corresponds to an A-scan rate of 416 kHz. For *in vivo* measurements of a human fingertip, the collimated beam had a width of 3.6 mm, and a high-speed CMOS camera (FASTCAM SA5, Photron USA, Inc.) was used with a measurement speed of 7000 fps and $1024 \times 1024$ pixels of size $20\,\mu\text{m} \times 20\,\mu\text{m}$. The sweep rate was adjusted accordingly to 350 nm/s. At this sweep rate, most motion artifacts could be prevented, if the fingertip was stabilized by a glass plate.

The imaging distance with both cameras (8.0 and 14 cm) was able to resolve all spatial frequencies of the holograms [12]. This resulted in effective NAs of 0.05 and 0.07, respectively, which correspond to Gaussian beam diameters ($2w_0$) of 10 or 7 $\mu$m and Rayleigh lengths ($2z_R$) of 200 or 100 $\mu$m. For comparison, confocally scanned OCT images were acquired at 910 nm with a spectrometer based system using a Basler runner ruL2048-30gm to acquire the spectra and a two-axis scanner with an NA of 0.06. The depth resolution was 5.4 $\mu$m in air at a full measurement depth of 2.7 mm.

For each acquired digital hologram, the holographic image was reconstructed for a specific reconstruction distance by multiplication with the conjugated reference wave and propagation of the light waves by the angular spectrum approach [7]. An additional magnification was introduced in the measurements by inserting a numerical lens [12] in order to achieve a pixel spacing of the reconstructed tomograms that is smaller than the diffraction-limited resolution.

After calculating the object wave field for all 1024 wavelengths, we have a data set that is similar to the data of a swept-source FF-OCT. Thus, a subsequent standard FD-OCT evaluation on the reconstructed holograms (i.e., an FFT with respect to the wavenumber axis with additional pre- and postprocessing) gave the same depth information as in standard FD-OCT. The reconstructed volume had a focus with diffraction-limited lateral resolution in the plane corresponding to the chosen reconstruction distance. By repeating this procedure for a number of planes with different distances, a complete volume was built up with the same diffraction-limited resolution in all planes and a depth-invariant sensitivity. The data were reconstructed on a high-performance PC utilizing four Opteron 6180 processors with 12 cores each. The processing time for a volumetric reconstruction of $1024 \times 1024 \times 512$ pixels with a single focus position was approximately 22 s.

The increased depth range of the holoscopy was demonstrated by imaging an OCT phantom for PSF measurements that was built from polyurethane resin doped with a low density of 300–800 nm sized red iron oxide nanoparticles [13]. Reconstruction in one distance provided good lateral resolution only in a restricted depth range [Figs. 2(a)–2(c)]. Additionally, the holographic dataset was reconstructed at five different focus positions, each 500 $\mu$m apart, and the focal regions were composed to one image. For this image, the lateral resolution is similar over a depth of more than 30 Rayleigh lengths [Fig. 2(d)]. A scanned confocal OCT of the same phantom with almost the same NA shows structures only over less than 1 mm with a strong roll-off of the signal intensity due to confocal gating [Fig. 2(e)].

Image quality was good enough to image the skin of a fingertip (Fig. 3) as long as a high-speed camera such as the Photron FASTCAM SA5 is used. With 7.3 million A scans, or seven volumes per second, this is to our knowledge the fastest area camera based OCT measurement presented yet. Even at this extreme speed, the sweep rate is almost 5 orders of magnitude lower than in commercial SS-OCT systems. Therefore, holoscopy is more sensitive to motion-induced image blurring than scanning FD-OCT systems. The ducts of the sweat glands [arrows in Figs. 3(a) and 3(b)] and the border between the horny layer and epidermis are visible with good contrast. The bright lines that appear in two depths are caused by multiple reflections at a window directly in front of the camera chip. In general, holoscopic images of scattering samples appeared less sharp than similar scanned images, which may be caused by residual noncompensated phase errors and multiple scattered photons.

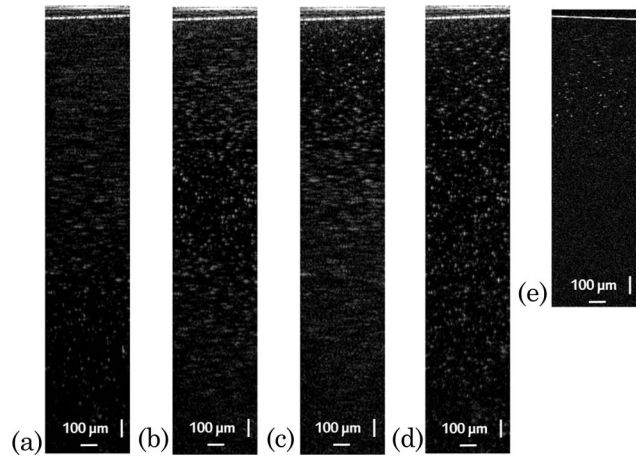


Fig. 2. Comparison of cross-sectional images taken from an OCT phantom by holoscopy and conventional scanning OCT. (a)–(c) Reconstruction of the holoscopic data for image planes of three different depths. (d) Fusion of the focal ranges of holoscopic reconstructions in five virtual focus positions, each 500 $\mu$m apart. The NA of the holoscopic images was 0.05. (e) Conventional B scan of the phantom at NA 0.06. The scale bars correspond to 0.1 mm.

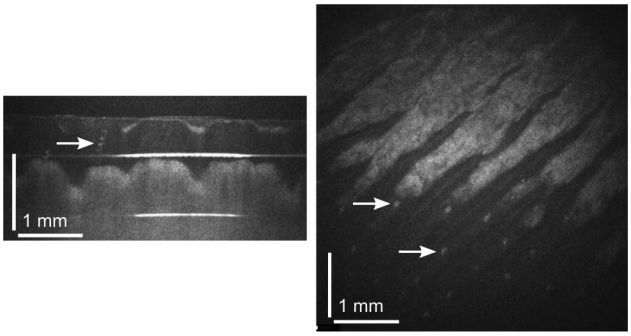


(a) (b)

Fig. 3. Holoscopic images of a fingertip. The focus for numerical reconstruction was put in the layer of the perspiratory glands. (a) One cross-sectional image and (b) one en-face image from the reconstructed data cuboid are shown. Dashed lines show the position of the slices. Media 1 shows an animated image of the three orthogonal planes of the reconstructed volume, and Media 2 shows a 3D rendering.

Though the holoscopic images still suffer from a lower image quality compared to commercial confocal scanning OCT systems, and some image artifacts are still present, the increase in imaging depth and the possibility of *in vivo* imaging were clearly demonstrated. Holoscopy is a viable alternative to standard OCT. Because of numerical refocusing techniques, each part of the image can be brought to focus with diffraction-limited resolution, and the origin of all single scattered (ballistic) photons can be determined. No photons from the sample are wasted by confocal gating, and a depth-invariant imaging quality, with respect to sensitivity and resolution, is possible. Compared to a full-field FD-OCT [11,14], the setup needs less optical elements, which reduces internal reflections, image artifacts, and aberrations. Sensitivity and axial resolution of standard swept-source FF-OCT systems are maintained. Because holoscopy is a very young technology, it is difficult to predict its impact on OCT and optical coherence microscopy. Advantages are especially obvious at a high imaging NA with a Rayleigh length much shorter than the depth of the image volume. Currently we are working on ultra-high-resolution holoscopy for imaging biopsies and other static samples where motion artifacts are not a problem. If sufficiently fast cameras are available, high-resolution imaging of the anterior section of the eye or even the complete eye could also be possible.

We thank the National Physical Laboratory, UK, for providing the OCT-phantom and Antje Klinger for the image visualization of OCT images with Imaris. This work was partly supported by the European Union (EU) Seventh Framework Programme (201880 FUN OCT).

**References**

1. J. Holmes, Proc. SPIE **7139**, 713908 (2008).
2. R. A. Leitgeb, M. Villiger, A. H. Bachmann, L. Steinmann, and T. Lasser, Opt. Lett. **31**, 2450 (2006).
3. T. S. Ralston, D. L. Marks, P. S. Carney, and S. A. Boppart, Nat. Phys. **3**, 129, doi:10.1038/nphys514 (2007).
4. T. S. Ralston, D. L. Marks, P. S. Carney, and S. A. Boppart, Opt. Express **16**, 2555 (2008).
5. L. Yu, B. Rao, J. Zhang, J. Su, Q. Wang, S. Guo, and Z. Chen, Opt. Express **15**, 7634 (2007).
6. D. L. Marks, T. S. Ralston, S. A. Boppart, and P. S. Carney, J. Opt. Soc. Am. A **24**, 1034 (2007).
7. M. K. Kim, SPIE Rev. **1**, 018005 (2010).
8. P. Blazkiewicz, M. Gourlay, J. R. Tucker, A. D. Rakic, and A. V. Zvyagin, Appl. Opt. **44**, 7722 (2005).
9. D. V. Shabanov, G. V. Geliknov, and V. M. Gelikonov, Laser Phys. Lett. **6**, 753 (2009).
10. M. C. Potcoava and M. K. Kim, Meas. Sci. Technol. **19**, 074010 (2008).
11. T. Bonin, G. Franke, M. Hagen-Eggert, P. Koch, and G. Hüttmann, Opt. Lett. **35**, 3432 (2010).
12. U. Schnars and W. P. O. Jüptner, Meas. Sci. Technol. **13**, R85 (2002).
13. P. D. Woolliams, R. A. Ferguson, C. Hart, A. Grimwood, and P. H. Tomlins, Appl. Opt. **49**, 2014 (2010).
14. B. Považay, A. Unterhuber, B. Hermann, H. Sattmann, H. Arthaber, and W. Drexler, Opt. Express **14**, 7661 (2006).